Assorted kerosene-based nanofluid across a dual-zone vertical annulus with electroosmosis

Sara I. Abdelsalam

A. M. Alsharif

Y. Abd Elmaboud

A. I. Abdellateef

Journal Pre-proof

Assorted kerosene-based nanofluid across a dual-zone vertical annulus with electroosmosis

Sara I. Abdelsalam, Abdullah Madhi Alsharif, Y. Abd Elmaboud and A.I. Abdellateef

This is a PDF file of an article that has undergone enhancements after acceptance, such as the addition of a cover page and metadata, and formatting for readability, but it is not yet the definitive version of record. This version will undergo additional copyediting, typesetting and review before it is published in its final form, but we are providing this version to give early visibility of the article. Please note that, during the production process, errors may be discovered which could affect the content, and all legal disclaimers that apply to the journal pertain.

Assorted kerosene-based nanofluid across a dual-zone vertical annulus with electroosmosis

Sara I. Abdelsalam[a,b,1], **Abdullah Madhi Alsharif**[c], **Y. Abd Elmaboud**[d,e,2], **A. I. Abdellateef**[f]

[a]Instituto de Ciencias *Matemáticas* ICMAT, CSIC, UAM, UCM, UC3M, Madrid 28049, Spain.

[b]Basic Science, Faculty of Engineering, The British University in Egypt, Al-Shorouk City, Cairo 11837, Egypt,

[c]Department of Mathematics and Statistics, College of Science, Taif University, P.O. Box 11099, Taif 21944, Saudi Arabia,

[d]University Of Jeddah, College of Science and Arts at Khulis, Department of mathematics, Jeddah, Saudi Arabia,

[e]Mathematics Department, Faculty of Science, Al-Azhar University (Assiut Branch), Assiut 71254, Egypt.

[f]Department of Applied Mathematics and Science, Faculty of engineering, National University of Science and Technology, Seeb 111, Sultanate of Oman.

Abstract: The goal of this numerical simulation is to visualize the electroosmotic flow of immiscible fluids through a porous medium in vertical annular microtubes. The inner region (Region I) is filled with an electrically conducting hybrid nanofluid while an electrically conducting Jeffrey fluid is flowing in the second region (Region II). The chosen nanofluid is kerosene-based and the nanoparticles (Fe_3O_4-TiO_2) are of a spherical shape. A strong zeta potential is taken into account and the electroosmotic velocity in the two layers is considered too. The annular microtubes are subjected to an external magnetic field and an electric field. The linked nonlinear governing equations with initial, interface and boundary conditions are solved using the finite difference method. The wall zeta potential and EDL thickness on the electric potential distribution, the velocity profile, the volumetric flow rate and the heat transfer are investigated versus the parameters under consideration. Graphs have been used to describe the numerical results of numerous emerging factors. It has been noticed that the temperature is the least for the clear fluid than the that of the non-clear one. Due to the fact that oil-based nanofluids are utilized to improve the stability and thermophysical characteristics of nanofluids when they are subjected to high temperatures, the proposed study presents a mathematical assessment that is sought to be useful in oil-based nanoflows' applications.

Keywords: Immiscible fluid; kerosene-based nanofluid; zeta potential; electroosmosis; annular region; magnetic field.

---

[1]**Corresponding author:** sara.abdelsalam@bue.edu.eg (Sara I. Abdelsalam)

[2]E-mail: yass_math@yahoo.com (Y. Abd Elmaboud)

	NOMENCLATURE
B_0	Magnetic field component [T]
E_0	Electric field component [v/m]
E	Electric field parameter
Ec	Eckert number
Gr	Grashof number
Ha	Hartmann number
p	Pressure [$\frac{N}{m^2}$]
P_r	Prandtl number
q'	Electroosmotic velocity [m/s]
$Q'(t')$	Instantaneous volume flow rate [m^3/s]
r	Radial direction [m]
$R_{1,2}$	Inner and outer radii [m]
T	Fluid temperature [K]
t'	The time [s]
$T_1 \& T_2$	Inner and outer tubes temperature [K]
v_s	Helmholtz-Smoluchowski velocity[m/s]
α_f	Thermal conductivity for fluid [W/(m K)]
α_R	Thermal conductivity ratio
α_{hnf}	Thermal conductivity of the hybrid nano-fluid [W/(m K)]
β_{hnf}	The thermal expansion coefficient of the hybrid nanofluid [(1/K)]
ξ_1, ξ_2	Surface electric charge for the inner and outer walls respectively [$C.m^{-2}$]
θ	Dimensionless temperature
κ	Debye-Hückle parameter
λ	Porosity parameter
λ_1	Permeability [m^2]
μ_R	Viscosity ratio
μ_{hnf}	Viscosity of the hybrid nano-fluid [$kg\ m^{-1}s^{-1}$]
ρ_{hnf}	Hybrid nanofluid density [kg/m^3]
ϱ_i	Charge density [$C.m^{-2}$]
σ_{hnf}	Electrical conductivity of the hybrid nanofluid [$kg^{-1}m^{-3}s^3A^2$]
$\varphi_{Fe_3O_4}$	Magnetite volume fraction
φ_{TiO_2}	Titanium oxide volume fraction
ψ'_i	Potential distribution [V]

2

1 Introduction

In the recent century, microfluidics have been an important tool due to its several applications for microfluidic devices, including drug delivery and other areas of medicine [1–4]. The pressure-driven technique has been widely employed for microscale mechanical pumping in a variety of engineering applications [5–7]. As the length scale of micro-fluidic devices has decreased, various features have appeared in the micro-fluidic flow exclusively driven by the pressure actuation mechanism, such as the dispersion of biomedical and the waste of energy [8]. The electro-osmotic flow (EOF) demonstrates a unique and superior ability to control liquid flows. It has been pointed out that this occurrence has some connection to the electric double layer (EDL), which is produced as a consequence of the ionized interaction with the charged wall in order to produce the charged precipitate. It is known that the electric field changes water structure in C-S-H nanopore and weakens the hydrophilicity and chloride ions adsorption [9]. Taking into account the application of the external electric field, the mobile ions in the EDL have a tendency to migrate and generate a fluid body force, which enables a bulk liquid to move through a viscous effect. Numerous experimental, theoretical and numerical studies on the EOF for different kinds of fluids have been published in the literature [10–27]. Modern technology has increased interest in flow and heat transfer research, which encompass heat exchangers, fluid transport, chemical processing equipment, and micro-electronic cooling. Many researchers with diverse hypotheses studied the problem of fluid flow and heat transfer [28–35]. Those investigations are single-fluid models. Most petroleum, plasma, magneto fluid, etc. issues require multifluid flow. Adding a second immiscible fluid phase to a fluid flow model complicates interactions between transport processes and the conditions at the interfaces between phases. A modest number of studies have been done on the movement of immiscible fluids. Vajravelu [36] conducted research on the unsteady flow that occurs when two immiscible conducting fluids are sandwiched between two permeable beds. Hibara et al. [37] investigated a microchip with a multilayer system in which the connecting medium and liquids were placed parallel to the lateral wall. Packham and Shail [38] looked at the stratified flow of two non-homogeneous liquids in a horizontal pipe. There are many papers in the literature discussed the idea of immiscible fluids [39–43]. In a wide range of engineering applications, including heat exchangers, fuel cells and similar devices, fluids play a critical role in accelerating the speed of heat transfer. In the process of heat transmission, normal fluids have an exceptionally poor thermal conductivity. Therefore, we need unconventional fluids with a high thermal conductivity so that we can solve this issue. Nanofluids are the name given to this particular kind of fluid. Choi [44] was the first to demonstrate a viable use for nanofluids. Nanofluids have a higher thermal conductivity than conventional fluids due to the inclusion of metal nanometer-sized particles, which is an important factor in raising thermal conductivity for that fluid movement and heat transfer that have been the primary focus of most researches, whether they have utilized regular fluid or nanofluid. Recently, there is a new class of nanofluids which is a hybrid nanofluid. This class consists of dual distinct nanoparticle suspension in the base fluid. Kerosene is used much as a base fluid in most hybrid nanofluid [45–47]. Dogonchi and Ganji [48] explored buoyant flow and heat transmission of MHD nanofluid on a stretched surface and

they concluded that when the radiation parameter is raised, the temperature and velocity of the fluid fall, which indicate a direct correlation between a drop in nanofluid volume percentage and an increase in the coefficient of skin friction. Entropy production on non-Newtonian Eyring-Powell nanofluids have been discussed by Bhatti et al. [49]. They found that the more suction leads the higher velocity. Additionally, their findings reveal that thermophoresis parameters and Brownian motion considerably enhance the temperature profile. Recently, there are many papers in the literature discussed hybrid nanofluid [50,51]. Motivated by the above literature, it has been noticed that the analysis of the unsteady electroosmotic flow of immiscible fluids has not been given full consideration. In this article, we are going to investigate the unsteady electroosmotic flow of immiscible fluids in a vertical annulus. The high zeta potential is taken into consideration. The finite difference method is used to solve the coupled nonlinear governing equations. The numerical outcomes of several emerging parameters have been discussed through graphs.
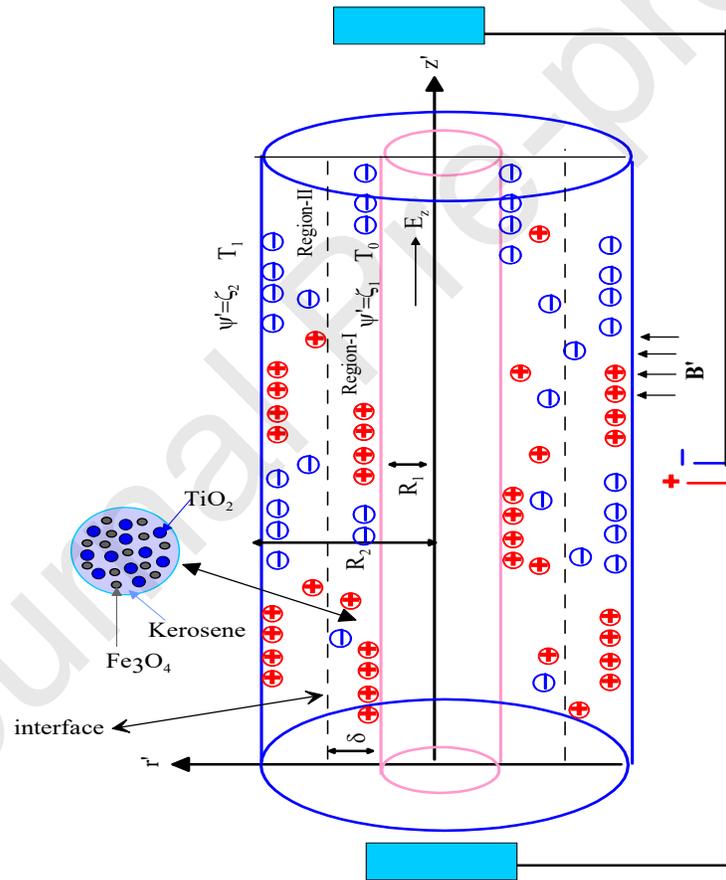

Figure 1: Geometrical configuration.

2 Problem Formulation

Let us consider an asymmetric immiscible electrolyte solution flow through a porous medium in vertical annular microtubes (Fig. 1) whose inner and outer radii are $r' = R_1$ and $r' = R_2$, respectively. The zeta potentials ($\xi_1 \& \xi_2$) represent a surface electric charge for the inner and outer walls respectively. The inner region (I) ($R_1 \leq r' \leq \delta'$) filled with an electrically conducting hybrid nanofluid (Fe_3O_4-TiO_2/ kerosene) while an electrically conducting Jeffrey fluid is flowing in the region (II) ($\delta' \leq r' \leq R_2$). Moreover, the inner tube is preserved at temperature T_0, while the outer one is preserved at temperature T_1.

2.1 Mathematical Model Assumptions

The following assumptions can be used to simplify the general governing equations presented in the current manuscript:

- The fluid physical qualities are unaffected by the temperature, ion concentration, or local electric field.

- Impermeable and flat interface between the fluids and ideally polarizable to electric charges.

- The annular microtubes is subjected to an external magnetic field $\mathbf{B} = (B_0, 0, 0)$ and electric field $\mathbf{E} = (0, 0, E_0)$.

- The electroosmotic velocity in the two layers is considered to be in the form $\mathbf{q}' = (0, 0, v'(r', t'))$ consequently the continuity equation is equally satisfied.

- The continuity of velocity, shear stress, temperature, and heat flux at the interface between the two fluid layers is considered.

- Gravitational force is taken into account and no overlap exists between the electric double layers.

- The Poisson equation combining between ψ' and ϱ_i', can be expressed as:

$$\frac{d^2 \psi_i'}{dr'^2} + \frac{1}{r'} \frac{d\psi_i'}{dr'} = \frac{-\varrho_i'}{\varepsilon}, \tag{1}$$

    where

$$-2ez_0 n_0 \sinh(\frac{ez_0 \psi_i'}{k_c T_c}) = \varrho_i' \tag{2}$$

    where $i = 1, 2$, stands for the two layers.

2.2 Governing Equations

The governing equations will be ([19], [20] and [42]):

Region-I-Hybrid nanofluid

$$\rho_{hnf} \frac{\partial v_1'}{\partial t'} = -\frac{\partial p'}{\partial x'} + \mu_{hnf} \left[\frac{1}{r'} \frac{\partial}{\partial r'} (r' \frac{\partial v_1'}{\partial r'}) \right] - \sigma_{hnf} B_0^2 v_1' - \frac{\mu_{hnf}}{\lambda_1} v_1' + E_x \varrho_1' + (\rho\beta)_{hnf} g(T_1' - T_0), \tag{3}$$

5

$$(\rho c_p)_{hnf}\frac{\partial T_1'}{\partial t'} = \alpha_{hnf}\Big\{\frac{\partial^2 T_1'}{\partial r'^2} + \frac{1}{r'}\frac{\partial T_1'}{\partial r'}\Big\} + \mu_{hnf}\big(\frac{\partial v_1'}{\partial r'}\big)^2 + \frac{\mu_{hnf}}{\lambda_1}v_1'^2 + \sigma_{hnf}B_0^2 v_1'^2 + \sigma_{hnf}E_x^2, \tag{4}$$

Region-II-Jeffrey fluid

$$\rho_f\frac{\partial v_2'}{\partial t'} = -\frac{\partial p'}{\partial x'} + \frac{\mu_f}{1+\chi}\Big[\frac{1}{r'}\frac{\partial}{\partial r'}(r'\frac{\partial v_2'}{\partial r'})\Big] - \sigma_f B_0^2 v_2' - \frac{\mu_f}{\lambda_1}v_2' + E_x\varrho_2' + (\rho\beta)_f g(T_2' - T_0), \tag{5}$$

$$(\rho c_p)_f\frac{\partial T_2'}{\partial t'} = \alpha_f\Big\{\frac{\partial^2 T_2'}{\partial r'^2} + \frac{1}{r'}\frac{\partial T_2'}{\partial r'}\Big\} + \frac{\mu_f}{1+\chi}\big(\frac{\partial v_2'}{\partial r'}\big)^2 + \frac{\mu_f}{\lambda_1}v_2'^2 + \sigma_f B_0^2 v_2'^2 + \sigma_f E_x^2, \tag{6}$$

where χ is Jeffrey model parameter (the ratio of relaxation to retardation times), λ_1 is the permeability parameter, μ_{hnf} and α_{hnf} are the viscosity and thermal conductivity of the hybrid nanofluid. The hybrid nanofluid density is designated by:

$$\rho_{hnf} = \varphi_{Fe_3O_4}\rho_{Fe_3O_4} + \varphi_{TiO_2}\rho_{TiO_2} + (1-\varphi)\rho_{kerosene}, \tag{7}$$

where, $\varphi_{Fe_3O_4}$ and φ_{TiO_2} are Magnetite and Titanium oxide volume fraction respectively, $\varphi = \varphi_{Fe_3O_4} + \varphi_{TiO_2}$. The viscosity of the hybrid nanofluid is

$$\mu_{hnf} = \frac{\mu_f}{(1-\varphi)^{2.5}}. \tag{8}$$

The effective electrical conductivity:

$$\frac{\sigma_{hnf}}{\sigma_f} = \Bigg[1 + \frac{3\big(\sigma_{np} - 1\big)\varphi}{\Big[\big(\sigma_{np} + 2\big) - \big(\sigma_{np} - 1\big)\varphi\Big]}\Bigg], \tag{9}$$

where $\sigma_{np} = \frac{\varphi_{Fe_3O_4}\sigma_{Fe_3O_4} + \varphi_{TiO_2}\sigma_{TiO_2}}{\sigma_f}$.

The heat capacitance:

$$(\rho c_p)_{hnf} = \varphi_{Fe_3O_4}\rho_{Fe_3O_4}(c_p)_{Fe_3O_4} + \varphi_{TiO_2}\rho_{TiO_2}(c_p)_{TiO_2} + (1-\varphi)(\rho c_p)_{kerosene}, \tag{10}$$

the thermal expansion coefficient takes the following form:

$$(\rho\beta)_{hnf} = (\varphi\rho\beta)_{Fe_3O_4} + (\varphi\rho\beta)_{TiO_2} + (1-\varphi)(\rho\beta)_{kerosene}. \tag{11}$$

For low dense mixtures of (Fe_3O_4-TiO_2/ kerosene) with spherical particles, the effective thermal conductivity according to Maxwell model is represented by:

$$\frac{\alpha_{hnf}}{\alpha_{kerosene}} = \frac{(\alpha_{hp} + 2\alpha_{kerosene}) - 2\phi(\alpha_{kerosene} - \alpha_{hp})}{(\alpha_{hp} + 2\alpha_{kerosene}) + \phi(\alpha_{kerosene} - \alpha_{hp})}, \tag{12}$$

where

$$\alpha_{hp} = \frac{\varphi_{Fe_3O_4}\alpha_{Fe_3O_4} + \varphi_{TiO_2}\alpha_{TiO_2}}{\varphi},$$

the thermo-physical characteristic of the hybrid nanofluid is shown in table 1.

Consider the initial, interface and boundary conditions in following form:

$$v'_1 = v'_2 = 0, \ T'_1 = T'_2 = T_0, \qquad\qquad\qquad \text{at} \ \ t' = 0,$$

$$\psi'_1 = \xi'_1, \ v'_1 = 0, \quad T'_1 = T_0, \qquad\qquad\qquad \text{at} \ \ t' > 0, \ r' = R_1,$$

$$\psi'_2 = \xi'_2, \ v'_2 = 0, \quad T'_2 = T_1, \qquad\qquad\qquad \text{at} \ \ t' > 0, \ r' = R_2,$$

$$\begin{cases} v'_1 = v'_2, \ T'_1 = T'_2, \psi'_1 = \psi'_2 \\ \mu_{hnf}\dfrac{\partial v'_1}{\partial r'} = \dfrac{\mu_f}{1+\chi}\dfrac{\partial v'_2}{\partial r'} \\ \dfrac{d\psi'_1}{dr'} = \dfrac{d\psi'_2}{dr'}, \ \alpha_{hnf}\dfrac{\partial T'_1}{\partial r'} = \alpha_f\dfrac{\partial T'_2}{\partial r'}, \end{cases} \text{at} \ \ r' = \delta', \tag{13}$$

The volumetric flow rate is defined by:

$$Q'(t') = 2\pi \int_{R_1}^{\delta'} r'v'_1 dr' + 2\pi \int_{\delta'}^{R_2} r'v'_2 dr'. \tag{14}$$

Introducing the non-dimensional variables as follows:

$$r = \frac{r'}{R_2}, \ \delta = \frac{\delta'}{R_2}, \ \ t = \frac{\mu_1}{\rho_f R_2^2}t', \ v = \frac{v'}{v_s}, \ F = -\frac{R_2^2}{\mu_1 v_s}\frac{\partial p'}{\partial z'}$$

$$\kappa = R_2\kappa', \ (\psi_{(i)}, \xi_{(i)}) = \frac{1}{\psi_z}(\psi'_{(i)}, \xi'_{(i)}), \ \rho_e^{(i)} = \frac{R_2^2\rho_e'^{(i)}}{\psi_z\varepsilon_1}, \ \theta = \frac{T' - T_0}{T_1 - T_0}, \tag{15}$$

where $\psi_z = \frac{k_c T_c}{ez_0}$, $\kappa'^2 = \left(\frac{2e^2z^2n_0}{\varepsilon k_c T}\right)$, $v_s = -\frac{\varepsilon\psi_z E_x}{\mu_1}$ is the Helmholtz-Smoluchowski velocity, κ is the Debye-Hückle parameter or electrokinetic parameter. Using Eq. 15 in Eqs. (1–14), the non-dimensional governing equations with the corresponding boundary conditions will be:

Region-I-Hybrid nanofluid

$$\frac{d^2\psi_1}{dr^2} + \frac{1}{r}\frac{d\psi_1}{dr} = \kappa^2\sinh(\psi_1), \tag{16}$$

$$\rho_R\frac{\partial v_1}{\partial t} = F + \mu_R\left[\frac{1}{r}\frac{\partial}{\partial r}(r\frac{\partial v_1}{\partial r})\right] - \sigma_R Ha^2 v_1 - \frac{\mu_R}{\lambda}v_1 + \kappa^2\sinh(\psi_1) + (\rho\beta)_R G_r\theta_1, \tag{17}$$

$$P_r(\rho c_p)_R\frac{\partial\theta_1}{\partial t} = \alpha_R\left\{\frac{\partial^2\theta_1}{\partial r^2} + \frac{1}{r}\frac{\partial\theta_1}{\partial r}\right\} + P_r\mu_R E_c\left[(\frac{\partial v_1}{\partial r})^2 + \frac{1}{\lambda}v_1^2\right] + \sigma_R P_r E_c\left[Ha^2 v_1^2 + E^2\right], \tag{18}$$

Region-II-Jeffrey fluid

$$\frac{d^2\psi_2}{dr^2} + \frac{1}{r}\frac{d\psi_2}{dr} = \kappa^2\sinh(\psi_2), \tag{19}$$

$$\frac{\partial v_2}{\partial t} = F + \frac{1}{1+\chi}\left[\frac{1}{r}\frac{\partial}{\partial r}(r\frac{\partial v_2}{\partial r})\right] - Ha^2 v_2 - \frac{1}{\lambda}v_2 + \kappa^2\sinh(\psi_2) + G_r\theta_2, \tag{20}$$

$$P_r\frac{\partial\theta_2}{\partial t} = \left\{\frac{\partial^2\theta_2}{\partial r^2} + \frac{1}{r}\frac{\partial\theta_2}{\partial r}\right\} + P_r E_c\left[\frac{1}{1+\chi}(\frac{\partial v_2}{\partial r})^2 + \frac{1}{\lambda}v_2^2\right] + P_r E_c\left[Ha^2 v_2^2 + E^2\right], \tag{21}$$

the instantaneous volume flow rate will be defined by:

$$Q(t) = 2\pi \int_{\frac{R_1}{R_2}}^{\delta} rv_1 dr + 2\pi \int_{\delta}^{1} rv_2 dr. \tag{22}$$

The non-dimensional boundary and initial conditions become:

$$
\begin{aligned}
&v_1 = v_2 = \theta_1 = \theta_2 = 0, && \text{at } t = 0, \\[4pt]
&\psi_1 = \xi_1, \ v_1 = 0, \quad \theta_1 = 0, && \text{at } t > 0, \ r = \frac{R_1}{R_2}, \\[4pt]
&\psi_2 = \xi_2, \ v_2 = 0, \quad \theta_2 = 1, && \text{at } t > 0, \ r = 1,
\end{aligned}
\tag{23}
$$

$$
\left.\begin{aligned}
&v_1 = v_2, \ \theta_1 = \theta_2, \psi_1 = \psi_2 \\
&\mu_R \frac{\partial v_1}{\partial r} = \frac{1}{1+\chi}\frac{\partial v_2}{\partial r} \\
&\frac{d\psi_1}{dr} = \frac{d\psi_2}{dr}, \ \alpha_R \frac{\partial \theta_1}{\partial r} = \frac{\partial \theta_2}{\partial r},
\end{aligned}\right\} \text{at} \quad r = \delta,
$$

where the Non-dimensional variables are defined as $Ha = R_2 B_0 \sqrt{\frac{\sigma_f}{\mu_f}}$ is Hartmann number, $\lambda = \frac{\lambda_1'}{R_2^2}$ is porosity parameter, $E = \frac{R_2 E_z}{v_s}\sqrt{\frac{\sigma_f}{\mu_f}}$ is electric field parameter , Grashof number is $Gr = \frac{g(\rho\beta)_f R_2^2 (T_1 - T_0)}{\mu_f v_s}$, $P_r = \frac{(C_p\mu)_f}{\alpha_f}$ is Prandtl number of the fluid, Eckert number is $E_c = \frac{v_s^2}{(C_p)_f (T_1 - T_0)}$, $\mu_R = \frac{\mu_{hnf}}{\mu_f}$ is the viscosity ratio, $\alpha_R = \frac{\alpha_h nf}{\alpha_f}$ is the thermal conductivity ratio,

3   Numerical solution

In this part, the finite difference approach is suggested to solve the Eqs. (16–22). Firstly, let

$$
r_i = \Delta r * i, \ t_j = \Delta t * j \ where \ i = 0, 1, 2, ..., N_r \ and \ j = 0, 1, 2, ..., N_t
\tag{24}
$$

where N_r and N_t are positive integers, $\Delta r = (DisplacmentDomain)/N_r$ and $\Delta t = (TimeDomain)/N_t$ are the space and time steps, respectively. The numerical solution $v_{1,2}(r,t), \theta_{1,2}(r,t), \psi_{1,2}(r)$ at the mesh point (r_i, t_j) is denoted by $v_{1,2}(i,j), \theta_{1,2}(i,j), \psi_{1,2}(i)$. On using Eq. (24) with the finite difference approximations we get:

Region-I-Hybrid nanofluid

$$
\frac{\psi_1(i-1) + \psi_1(i+1) - 2\psi_1(i)}{(\Delta r)^2} + \frac{1}{\Delta r * i + r_0}\frac{\psi_1(i+1) - \psi_1(i-1)}{2 * \Delta r} = \kappa^2 \sinh(\psi_1(i)),
\tag{25}
$$

$$
\begin{aligned}
&\frac{\rho_R(v_1(i,j) - v_1(i,j-1))}{\Delta t} = F + \frac{\mu_R(v_1(i-1,j) + v_1(i+1,j) - 2v_1(i,j))}{\Delta r^2} + \frac{\mu_R}{\Delta r * i + r_0} \\
&\frac{v_1(i+1,j) - v_1(i-1,j)}{2 * \Delta r} - Ha^2(\sigma_R)v_1(i,j) - \frac{\mu_R}{\lambda_1}v_1(i,j) + \kappa^2\sinh(\psi_1(i,j)) + (\rho\beta)_R G_r\theta_1(i,j)
\end{aligned}
\tag{26}
$$

$$
\begin{aligned}
&P_r(\rho cp)_R\frac{\theta_1(i,j) - \theta_1(i,j-1)}{\Delta t} = \alpha_r\Big[\frac{\theta_1(i-1,j) + \theta_1(i+1,j) - 2\theta_1(i,j)}{\Delta r^2} + \frac{1}{(\Delta r * i + r_0)} \\
&\frac{\theta_1(i+1,j) - \theta_1(i-1,j)}{(2\Delta r)}\Big] + P_r E_r \mu_R\Big[\Big(\frac{v_1(i+1,j) - v_1(i-1,j)}{2\Delta r}\Big)^2 + \frac{v_1(i,j)^2}{\lambda_1}\Big] + \\
&\sigma_r P_r E_r\Big[E^2 + Ha^2(v_1(i,j))^2\Big]
\end{aligned}
\tag{27}
$$

Region-II-Jeffrey fluid

$$
\frac{\psi_2(i-1) + \psi_2(i+1) - 2\psi_2(i)}{(\Delta r)^2} + \frac{1}{\Delta r * i + r_0}\frac{\psi_2(i+1) - \psi_2(i-1)}{2 * \Delta r} = \kappa^2 \sinh(\psi_2(i)),
\tag{28}
$$

8

$$\frac{(v_2(i,j) - v_2(i,j-1))}{dt} = F + \frac{1}{1+\chi}\Big[\frac{(v_2(i-1,j) + v_1(i+1,j) - 2v_2(i,j))}{\Delta r^2} +$$

$$\frac{1}{\Delta r * i + r_0}\frac{v_2(i+1,j) - v_2(i-1,j)}{2 * \Delta r}\Big] - Ha^2 v_2(i,j) - \frac{1}{\lambda_1}v_2(i,j) + \kappa^2 \sinh(\psi_1(i,j)) + G_r\theta_1(i,j) \qquad (29)$$

$$P_r\frac{\theta_2(i,j) - \theta_2(i,j-1)}{dt} = (\frac{\theta_2(i-1,j) + \theta_2(i+1,j) - 2\theta_2(i,j)}{\Delta r^2} + \frac{1}{(\Delta r * i + r_0)}$$

$$\frac{\theta_2(i+1,j) - \theta_2(i-1,j)}{(2\Delta r)}) + P_rE_r\Big[\left(\frac{v_1(i+1,j) - v_1(i-1,j)}{2\Delta r}\right)^2 + \frac{v_1(i,j)^2}{\lambda_1}\Big] + \qquad (30)$$

$$P_rE_r\Big[E^2 + Ha^2(v_1(i,j))^2\Big]$$

The boundary and initial conditions Eq. (23) can be discredited as:

$$v_1(i,0) = v_2(i,0) = \theta_1(i,0) = \theta_2(i,0) = 0, \qquad\qquad \text{at } t = 0,$$

$$\psi_1(r) = \xi_1,\ v_1(r,\mathrm{j}) = 0,\quad \theta_1(r,\mathrm{j}) = 0, \qquad\qquad \text{at } t > 0,\ r = \frac{R_1}{R_2},$$

$$\psi_2(1) = \xi_2,\ v_2(1,\mathrm{j}) = 0,\quad \theta_2(1,\mathrm{j}) = 1, \qquad\qquad \text{at } t > 0,\ r = 1,$$

$$\begin{cases} v_1(\delta,j) = v_2(\delta,j),\ \theta_1(\delta,j) = \theta_2(\delta,j),\ \psi_1(\delta) = \psi_2(\delta) \\ \mu_R\Big[v_1(\delta,j) - v_1(\delta-1,j)\Big] = \frac{1}{1+\chi}\Big[v_2(\delta+1,j) - v_2(\delta,j))\Big] \\ \psi_1(\delta) - \psi_1(\delta-1) = \psi_2(\delta+1) - \psi_2(\delta),\ \alpha_R\Big[\theta_1(\delta,j) - \theta_1(\delta-1,j)\Big] = \theta_2(\delta+1,j) - \theta_2(\delta,j)) \end{cases} \text{at}\quad r = \delta.$$

$$(31)$$

Finally, the nonlinear algebraic equations (Eqs. (25–31)) are solved at each iterative step to get numerical results of $v_{1,2}(i,j), \theta_{1,2}(i,j), \psi_{1,2}(i)$.

4 Graphical results and discussion

The aim of this section is to investigate the influences of the pertinent parameters on the wall zeta potential and EDL thickness on the electric potential distribution, velocity distribution and heat transfer. The numerical solution is derived for the unsteady flow of the immiscible fluid in the vertical annulus with electroosmosis to serve that purpose. The comparisons of behaviors of the physical variables are set between region I that represents the hybrid nanofluid and region II that represents the Jeffrey fluid model. First of all, the grid independence test should be essentially presented in order to ensure that simulation results are not affected by the grid size. To achieve that, Figure 2 is plotted to discuss the variations in the grid independence test with various mesh sizes for the velocity and heat transfer for different values of the other parameters in interest. It is seen from the velocity profile in Fig. 2a that flow accelerates in the hybrid nanofluid region whereas it has a sharp decrease after a moderate increase in the non-Newtonian fluid region. It is also seen that the flow tends to have a parabolic shape in the non-Newtonian region. Based on the grid independence test for the model presented in Fig. 2b, it is seen that the heat transfer is almost negligible for the hybrid nanofluid comparing to the Jeffrey fluid which is seen to be increasing steadily with an increase in the mesh size. For both the velocity and heat transfer and on the basis of the grid independence test, it is shown that the mesh element of the given size or less

has an incremental effect and is not affecting the results. Hence, the mesh element of the shown size in Figure 2 is considered for the ongoing analysis.

4.1 Wall zeta potential and EDL thickness on the electric potential distribution

Figure 3 presents the variations of the electric potential distribution for various values of κ with varying zeta potentials. It is elucidated in Fig. 3a that κ has a decreasing effect on the electric potential profile for both hybrid nanofluid and non-Newtonian fluid with symmetric zeta potentials ($\xi_1 = 1$ and $\xi_2 = 1$). It is also observed that the electric potential decreases progressively with r for the hybrid nanofluid while an opposite behavior is shown for the Jeffrey fluid. A different behavior is shown in Fig. 3b for the electric potential distribution with asymmetric zeta potentials ($\xi_1 = -1$ and $\xi_2 = 1$). A curve exhibiting a plateau between the steeply ascending sections (regions I and II) is observed. It is shown that κ acts as an enhancing factor for the electric potential in the hybrid nanofluid region, whereas it acts as a decaying factor for the electric potential in the Jeffrey fluid region. It is seen that the asymmetry of zeta potentials allows the presence of a non-uniform velocity profile which confirms with the results found by Medina et al. [11].

4.2 Velocity

The velocity characteristics are illustrated in Figs. (4–9) for various values of the parameters under consideration in the hybrid nanofluid and Jeffrey fluid region for $t = 1$. Figure 4 demonstrates the effect of the volume fraction φ on the velocity profile with varying values of the other parameters for clear and non-clear fluid. It is observed that φ causes the fluid to decelerate for the hybrid nanofluid region and for the Jeffrey flow region. It is also shown that the velocity profile attains higher values for the clear fluid than that the non-clear fluid in both fluid regions. Figure 5 elucidates the variations of velocity for different values of κ with varying r for asymmetric zeta potentials. It is noticed that the flow shows an anti-symmetry behavior that contains maximum and minimum when zeta potentials are not equal. The non-monotony in the velocity distribution across the annulus is seen to be attributed with the asymmetric zeta potentials for both the hybrid nanofluid and Jeffrey flow regions. Figure 6 is plotted to observe the variations of the velocity profile, that is plotted versus r, with various values of the Jeffrey fluid parameter, χ. It is seen that the flow accelerates with an increase in χ for various values of the pertinent parameters. The reason behind this phenomenon is that the elastic materials exhibit an instantaneous deformation. Figure 7 (a,b) gives a thorough description to the behavior of flow with Grashof number across the annulus for the symmetric case when $\xi_1 = \xi_2 = 1$. It is obvious that the flow profile increases uniformly with time through the annulus reaching a plateau in all regions and for both hybrid and Jeffrey fluids. Figure 8 demonstrates the impact of the porosity parameter λ on the velocity distribution where it is noticed that the flow is enhanced greatly with an increase λ. This is due to the resistance of the medium to the flow. Inversely, it is seen from Fig. 9 that the flow decelerates in both

10

regions with an increase in the Hartmann number Ha for the symmetric case. The declining trend in the velocity distribution is explained due to the dominating role of the retarding force in the flow field.

4.3 Heat transfer

The behavior of heat transfer θ across the vertical annulus for sundry values of the parameters of interest is demonstrated graphically through Figs. (10–14) for the symmetric case where $\xi_1 = 1$ and $\xi_2 = 1$. It is seen in Fig. 10 that φ has a decreasing effect on the heat transfer especially in the hybrid fluid region than that of the non-Newtonian region. It is also noticed that the temperature is the least for the clear fluid than the non-clear one in both regions. Figure 11 describes the behavior of θ that is plotted versus r for various values of χ where it is seen that θ increases progressively with increasing χ. It is noticed from Figs. 10 and 11 that θ is generally higher in the hybrid nanofluid region for various values of φ and χ. Figures 12 and 13 depict the behavior of θ, that is plotted along r, with varying κ and Ha, respectively, for different values of parameters of interest. It is evident that there is a gradual enhancement in the temperature profile till it reaches the maximum value in the Jeffrey flow region. It is noticed that both κ and Ha have an increasing effect on θ except for the small hybrid nanofluid region of $0.1 \leq r \leq 0.23$ with Ha where θ is seen to be reduced before an incremental effect of Ha on it in the same region. Figure 14 elucidates the behavior of θ, that is plotted versus t, with Eckert number Ec for various values of the pertinent parameters. It is observed that the temperature profile is highly dependent on Ec which is seen to be steeply enhancing θ with an increase in time.

4.4 Validation of results

To validate our results, we prepared Figure 15 to represent a comparison between the analytical solution [52] for electroosmotic clear fluid in a single zone and the numerical solution. The figure shows that the current results are very accurate.

5 Conclusion and Final Remarks

The unsteady electroosmotic flow of immiscible fluids in a vertical annulus will be investigated in this study. The strong zeta potential is taken into account. The linked nonlinear governing equations are solved using the finite difference method. Graphs have been used to describe the numerical results of numerous emergent factors. The most important findings found are as follows:

- The asymmetry of zeta potentials allows the presence of a non-uniform velocity profile which confirms with the results found by Medina et al. [11].

- The nonmonotonic distribution across the annulus is seen to be attributed with the asymmetric zeta potentials for both the hybrid nanoflow and Jeffrey flow regions.

- The flow decelerates with an increase in the Jeffrey parameter unlike the impact of the porosity parameter on it.

11

- The flow profile increases uniformly with time through the annulus reaching a plateau in all regions and for both hybrid and Jeffrey fluids.

- There is a gradual enhancement in the temperature profile till it reaches the maximum value in the Jeffrey flow region.

- The flow decelerates in both regions with an increase in the Hartmann number for the symmetric case.

- The temperature is the least for the clear fluid than the non-clear one in both regions.

- The temperature profile is seen to be steeply enhanced with an increase in time.

Author contribution statement:

Sara I. Abdelsalam; Abdullah Madhi Alsharif; Y. Abd Elmaboud; A. I. Abdellateef: Conceived and designed the experiments; Performed the experiments; Analyzed and interpreted the data; Contributed reagents, materials, analysis tools or data; Wrote the paper.

Data availability statement:

No data was used for the research described in the article.

Table (1): Thermo-physical characteristics of the nanoparticles Fe_3O_4, TiO_2 and the base fluid kerosene ([46, 47]).

Physical properties	kerosene	Fe_3O_4	TiO_2
$C_p\ [\frac{J}{kgK}]$	2090	670	686.2
$\rho\ [\frac{kg}{m^3}]$	783	5810	4250
$\alpha\ [\frac{W}{mK}]$	0.145	6	8.9538
$\beta\ [\frac{1}{K}]$	99*10^{-5}	$1.3*10^{-5}$	$0.84*10^{-5}$
$\sigma\ [\frac{1}{\Omega.m}]$	$6*10^{-10}$	25000	$0.24*10^7$
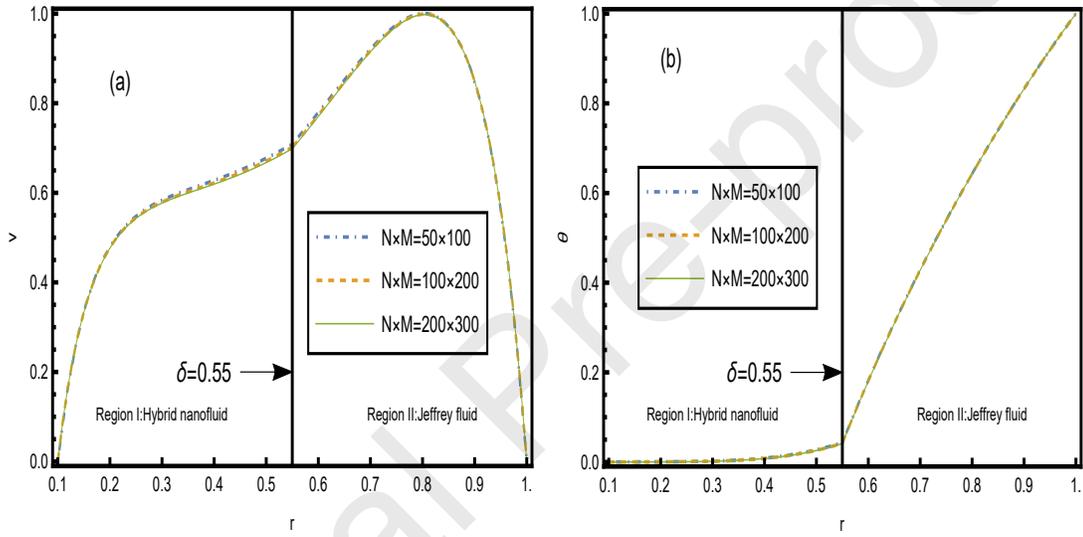
Figure 2: Grid independence test for different mesh sizes for the velocity and heat transfer at $\kappa = 10, \varphi = 6\%, F = -2, \ Ha = 2, E_c = 0.002, \lambda = 2, \ Gr = 5, P_r = 6.2, E = 1, \chi = 0, \xi_1 = 1, \xi_2 = 1, \ t = 1$.
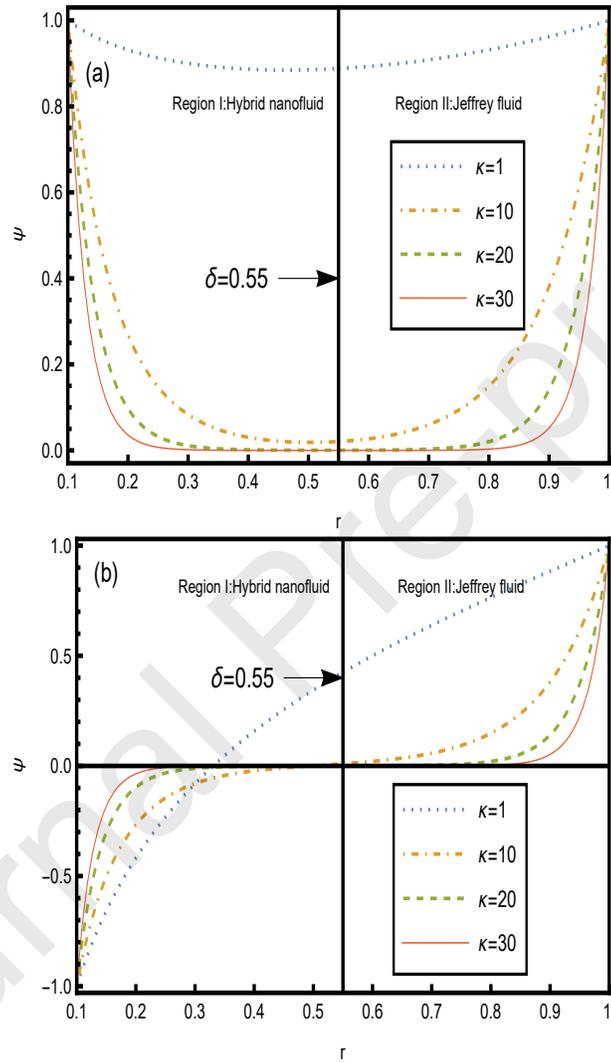
13

Figure 3: The electric potential distribution for different values of κ at $\xi_1 = 1, \xi_2 = 1$ (Panel (a)) and $\xi_1 = -1, \xi_2 = 1$ (Panel (b)).
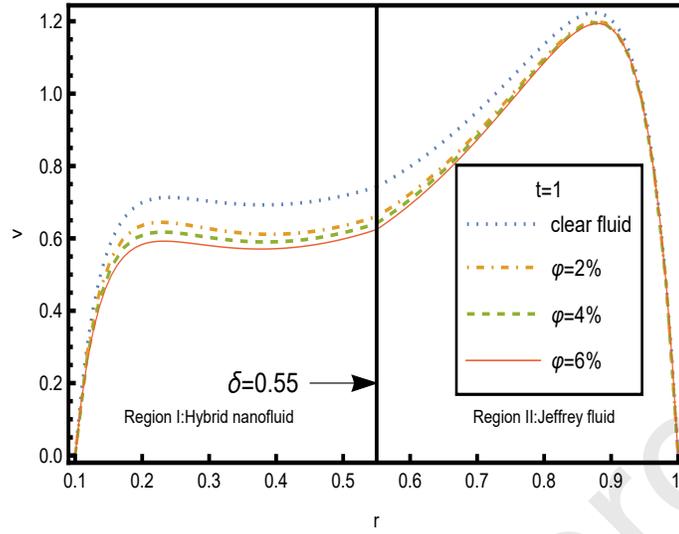
Figure 4: The velocity for different values of φ at $\kappa = 20, F = -2,\ Ha = 2, E_c = 0.002, \lambda = 2,\ Gr = 2, P_r = 6.2, E = 1, \chi = 0.8, \xi_1 = 1, \xi_2 = 1$.
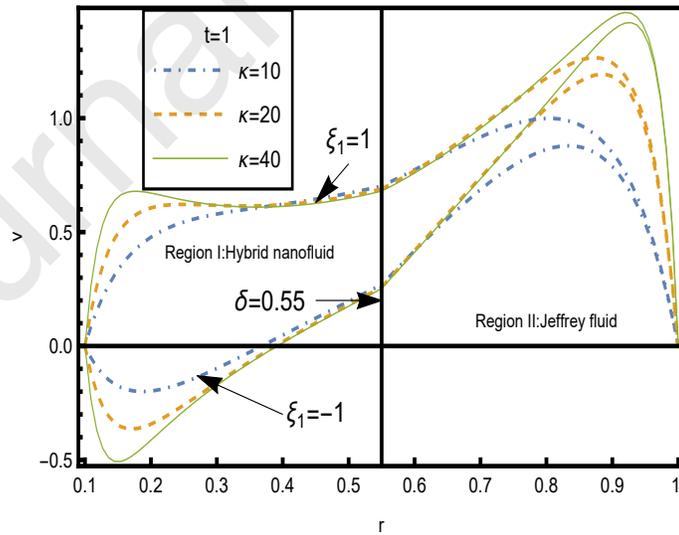
Figure 5: The velocity for different values of κ and ξ_1 at $\varphi = 6\%, F = -2,\ Ha = 2, E_c = 0.002, \lambda = 2,\ Gr = 5, P_r = 6.2, E = 1, \chi = 0, \xi_2 = 1$.

15
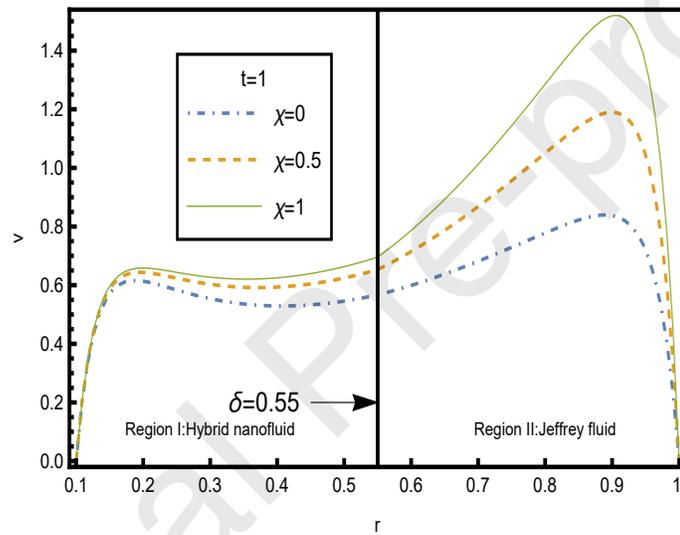
Figure 6: The velocity for different values of χ at $\kappa = 30, \varphi = 6\%, F = -2,\ Ha = 2, E_c = 0.002, \lambda = 2,\ Gr = 5, P_r = 6.2, E = 1, \xi_1 = 1, \xi_2 = 1$.
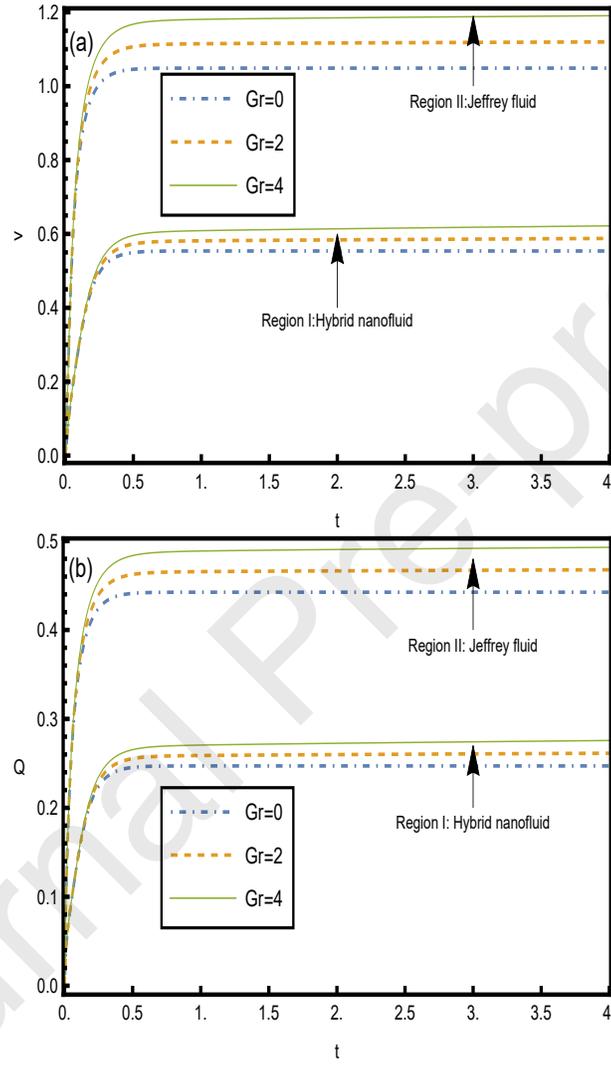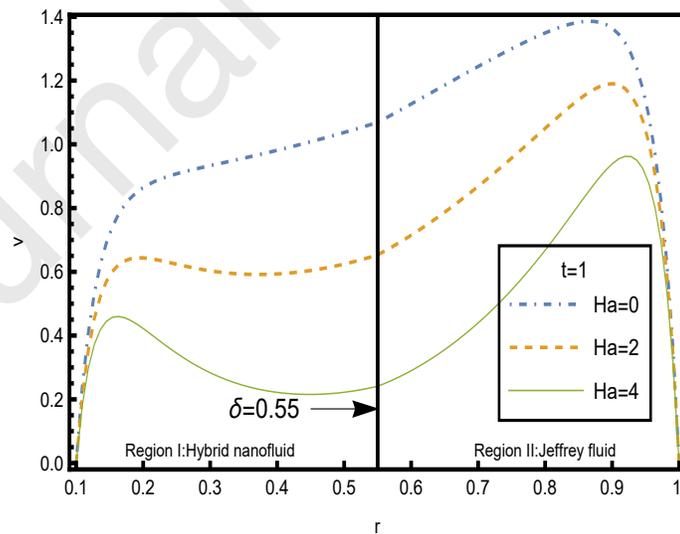
Figure 7: The velocity (Panel (a)) and the flow rate (Panel (b)) versus time for different values of Gr at $\kappa = 30, \varphi = 6\%, F = -2, \ Ha = 2, E_c = 0.002, \lambda = 2, \ \chi = 1, P_r = 6.2, E = 1, \xi_1 = 1, \xi_2 = 1$.

17
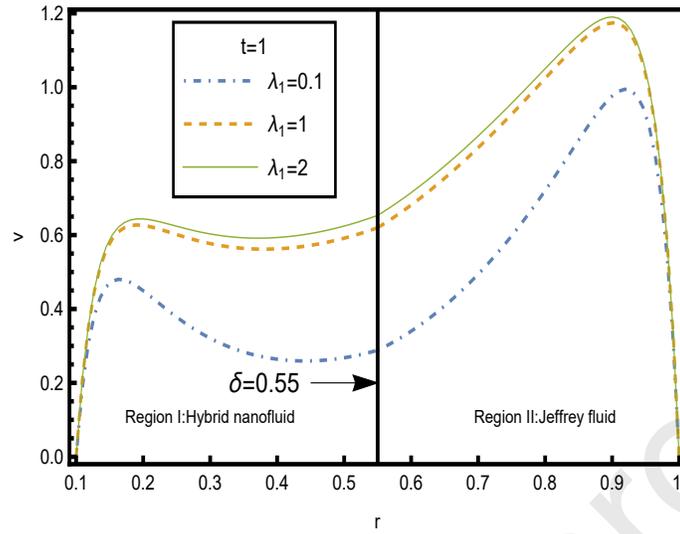
Figure 8: The velocity for different values of λ at $\kappa = 30, \varphi = 6\%, F = -2, \; Ha = 2, E_c = 0.002, \chi = 0.5, \; Gr = 5, P_r = 6.2, E = 1, \xi_1 = 1, \xi_2 = 1$.

Figure 9: The velocity for different values of Ha at $\kappa = 30, \varphi = 6\%, F = -2, \; \lambda = 2, E_c = 0.002, \chi = 0.5, \; Gr = 5, P_r = 6.2, E = 1, \xi_1 = 1, \xi_2 = 1$.
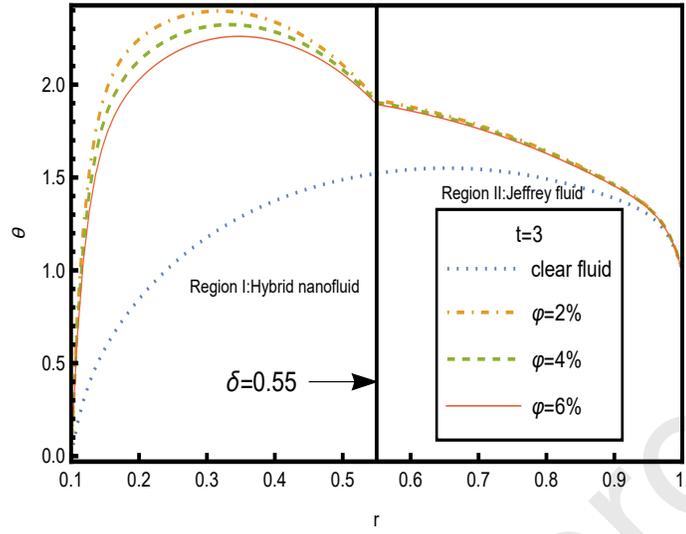
18

Figure 10: The heat transfer for different values of φ at $\kappa = 20, F = -2, \ Ha = 2, \ \lambda = 2, E_c = 0.2, \chi = 0.2, \ Gr = 2, P_r = 6.2, E = 1, \xi_1 = 1, \xi_2 = 1$.
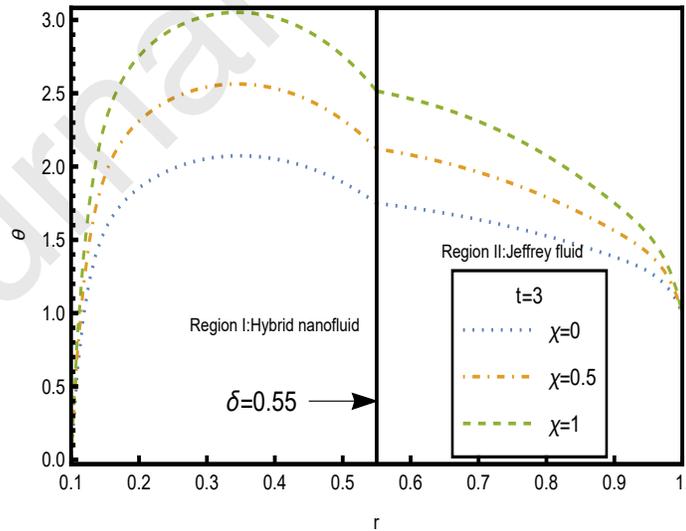

Figure 11: The heat transfer for different values of χ at $\kappa = 20, F = -2, \ Ha = 2, \ \lambda = 2, E_c = 0.2, \varphi = 6\%, \ Gr = 2, P_r = 6.2, E = 1, \xi_1 = 1, \xi_2 = 1$.
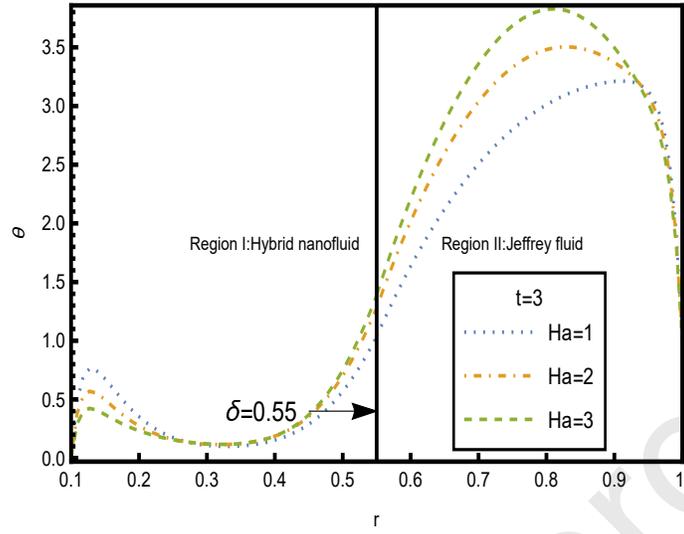
19

Figure 12: The heat transfer for different values of Ha at $\kappa = 20, F = -2, \chi = 0.5, \lambda = 2, E_c = 1, \varphi = 6\%, Gr = 2, P_r = 6.2, E = 1, \xi_1 = 1, \xi_2 = 1$.
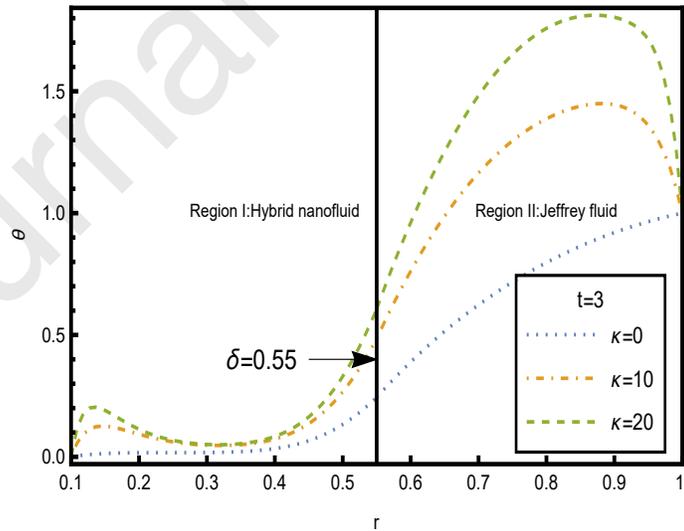

Figure 13: The heat transfer for different values of κ at $Ha = 2, F = -2, \chi = 0.5, \lambda = 2, E_c = 0.5, \varphi = 6\%, Gr = 2, P_r = 6.2, E = 1, \xi_1 = 1, \xi_2 = 1$.
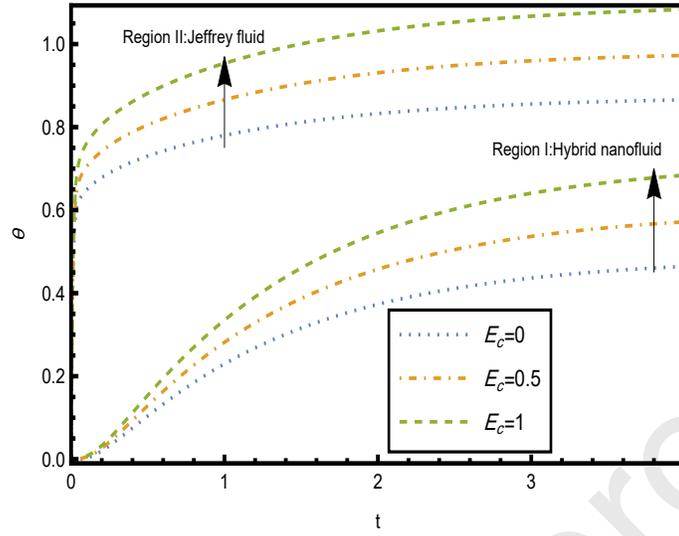
20

Figure 14: The heat transfer versus time t for different values of E_c at $Ha = 2, F = -2, \chi = 0.5, \ \lambda = 2, \kappa = 20, \varphi = 6\%, \ Gr = 2, P_r = 0.2, E = 1, \xi_1 = 1, \xi_2 = 1.$
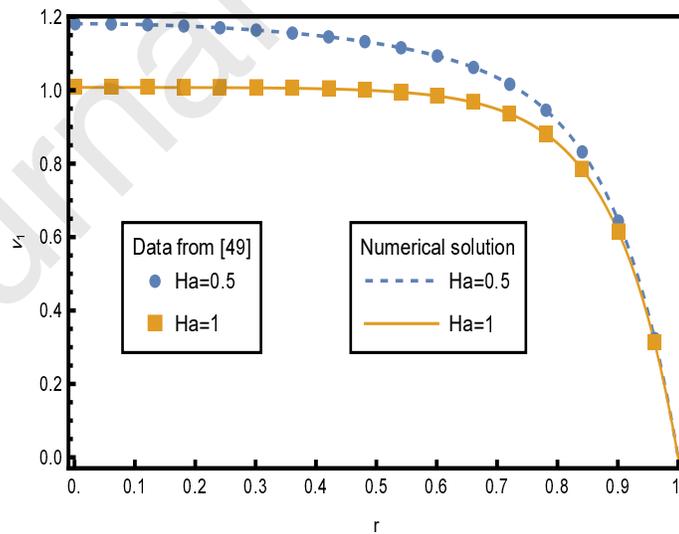

Figure 15: Comparisons of numerical solution and analytical solution [52] for different values of Ha at $F = 1, \kappa = 10, \xi_2 = 1.$

21

References

[1] P. Gravesen, J. Branebjerg, O.S. Jensen, Microfluidics-a review, J Micromech Microeng. 3 (1993) 168-182. https://doi.org/10.1088/0960-1317/3/4/002.

[2] H. Becker, C. Gärtner. Polymer microfabrication methods for microfluidic analytical applications, Electrophoresis. 21(2000)12-26, https://doi.org/10.1002/(SICI)1522-2683(20000101)21:1<12::AID-ELPS12>3.0.CO;2-7.

[3] B. Ziaie, Hard and soft micromachining for BioMEMS: review of techniques and examples of applications in microfluidics and drug delivery, Adv. Drug Deliv. Rev. 56 (2004) 145-172. https://doi.org/10.1016/j.addr.2003.09.001.

[4] K. Ohno, K. Tachikawa, A. Manz, Microfluidics: Applications for analytical purposes in chemistry and biochemistry, Electrophoresis. 29 (2008) 4443-4453. https://doi.org/10.1002/elps.200800121.

[5] S. Shoji, S. Nakagawa, M. Esashi, Micropump and sample-injector for integrated chemical analyzing systems, Sens. Actuator A Phys. 21 (1990) 189-192. https://doi.org/10.1016/0924-4247(90)85036-4.

[6] B.D. Iverson, S.V. Garimella, Recent advances in microscale pumping technologies: a review and evaluation, Microfluid Nanofluidics. 5 (2008) 145-174. https://doi.org/10.1007/s10404-008-0266-8.

[7] Z. Wu, N.-T. Nguyen, Hydrodynamic focusing in microchannels under consideration of diffusive dispersion: theories and experiments, Sens. Actuators B Chem. 107 (2005) 965-974. https://doi.org/10.1016/j.snb.2004.11.014.

[8] Z.-Y. Xie, Y.-J. Jian, Entropy generation of two-layer magnetohydrodynamic electroosmotic flow through microparallel channels, Energy. 139 (2017) 1080-1093. https://doi.org/10.1016/j.energy.2017.08.038.

[9] Y. Chen, M. Chen, X. Tong, S. Wang, X. Kang, Molecular insights into the interactions between chloride liquids and C S H nanopore surfaces under electric field-induced transport, J. Mol. Liq. 364 (2022) 119942. https://doi.org/10.1016/j.molliq.2022.119942.

[10] V.K. Narla, D. Tripathi, O.A. Bég, Electro-osmotic nanofluid flow in a curved microchannel, Chin J Phys. 67 (2020) 544-558, https://doi.org/10.1016/j.cjph.2020.08.010.

[11] I. Medina, M. Toledo, F. Méndez, O. Bautista, Pulsatile electroosmotic flow in a microchannel with asymmetric wall zeta potentials and its effect on mass transport enhancement and mixing, Chem. Eng. Sci. 184 (2018) 259-272, https://doi.org/10.1016/j.ces.2018.03.051.

[12] A.M. Alsharif, A.I. Abdellateef, Y.A. Elmaboud, S.I. Abdelsalam, Performance enhancement of a DC-operated micropump with electroosmosis in a hybrid nanofluid: fractional Cattaneo heat flux problem, APPL MATH MECH-ENGL. 43 (2022) 931-944. https://doi.org/10.1007/s10483-022-2854-6.

[13] J.G. Santiago, Electroosmotic Flows in Microchannels with Finite Inertial and Pressure Forces, Anal. Chem. 73 (2001) 2353-2365. https://doi.org/10.1021/ac0101398.

[14] D.G. Haywood, Z.D. Harms, S.C. Jacobson, Electroosmotic Flow in Nanofluidic Channels, Anal. Chem. 86 (2014) 11174-11180. https://doi.org/10.1021/ac502596m.

[15] X. Wang, H. Qi, B. Yu, Z. Xiong, H. Xu, Analytical and numerical study of electroosmotic slip flows of fractional second grade fluids, Commun Nonlinear Sci Numer Simul. 50 (2017) 77-87. https://doi.org/10.1016/j.cnsns.2017.02.019.

[16] X. Wang, H. Qi, H. Xu, Transient electro-osmotic flow of generalized second-grade fluids under slip boundary conditions, Can J Phys. 95 (2017) 1313-1320. https://doi.org/10.1139/cjp-2017-0179.

[17] J. Li, X. Si, B. Li, L. Cao, P. Zhang, The effects of depletion layer for electro-osmotic flow of fractional second-grade viscoelastic fluid in a micro-rectangle channel, Appl. Math. Comput. 385 (2020) 125409. https://doi.org/10.1016/j.amc.2020.125409.

[18] Q Liu, Y Jian, L Yang . Alternating current electroosmotic flow of the Jeffreys fluids through a slit microchannel. Phys. Fluids 23(2011)102001, https://doi.org/10.1063/1.3640082

[19] M. Zhao, S. Wang, S. Wei, Transient electro-osmotic flow of Oldroyd-B fluids in a straight pipe of circular cross section, J Nonnewton Fluid Mech. 201 (2013) 135-139. https://doi.org/10.1016/j.jnnfm.2013.09.002.

[20] F. Li, Y. Jian, Z. Xie, Y. Liu, Q. Liu, Transient alternating current electroosmotic flow of a Jeffrey fluid through a polyelectrolyte-grafted nanochannel, RSC Advances. 7 (2017) 782-790. https://doi.org/10.1039/c6ra24930b.

[21] V.K. Narla, D. Tripathi, D.S. Bhandari, Thermal analysis of micropolar fluid flow driven by electroosmosis and peristalsis in microchannels, Int. J. Ambient. Energy. 43 (2022) 8193-8205. https://doi.org/10.1080/01430750.2022.2091034.

[22] V.K. Narla, D Tripathi, D.S Bhandari, O. Anwar Bég. Electrokinetic insect-bioinspired membrane pumping in a high aspect ratio bio-microfluidic system, Microfluid Nanofluidics. 26(85)(2022), https://doi.org/10.1007/s10404-022-02588-2

[23] J. Akram, N.S. Akbar, D. Tripathi, Electroosmosis augmented MHD peristaltic transport of SWCNTs suspension in aqueous media, J. Therm. Anal. Calorim. 147 (2021) 2509-2526. https://doi.org/10.1007/s10973-021-10562-3.

[24] R. Choudhari, K. Ramesh, D. Tripathi, H. Vaidya, K.V. Prasad, Heat transfer and electroosmosis driven MHD peristaltic pumping in a microchannel with multiple slips and fluid properties, Heat Transfer. 51 (2022) 6507-6527. https://doi.org/10.1002/htj.22602.

[25] D.S. Bhandari, D. Tripathi, O. Anwar Bég, Electro-osmosis modulated periodic membrane pumping flow and particle motion with magnetic field effects, Phys. Fluids. 34 (2022) 092014. https://doi.org/10.1063/5.0111050.

[26] J. Akram, N.S. Akbar, D. Tripathi, Analysis of electroosmotic flow of silver-water nanofluid regulated by peristalsis using two different approaches for nanofluid, J Comput Sci. 62 (2022) 101696. https://doi.org/10.1016/j.jocs.2022.101696.

[27] T. Siva, B. Kumbhakar, S. Jangili, P.K. Mondal, Unsteady electro-osmotic flow of couple stress fluid in a rotating microchannel: An analytical solution, Phys. Fluids. 32 (2020) 102013. https://doi.org/10.1063/5.0023747.

[28] R.A. Alpher, Heat transfer in magnetohydrodynamic flow between parallel plates, Int. J. Heat Mass Transf. 3 (1961) 108-112. https://doi.org/10.1016/0017-9310(61)90073-4.

[29] H.A. Attia, N.A. Kotb, MHD flow between two parallel plates with heat transfer, Acta Mechanica. 117 (1996) 215-220. https://doi.org/10.1007/bf01181049.

[30] A.J. Chamkha, Unsteady laminar hydromagnetic fluid–particle flow and heat transfer in channels and circular pipes, Int J Heat Fluid Flow. 21 (2000) 740-746. https://doi.org/10.1016/s0142-727x(00)00031-x.

[31] M. Haajizadeh, C.L. Tien, Combined natural and forced convection in a horizontal porous channel, Int. J. Heat Mass Transf. 27 (1984) 799-813. https://doi.org/10.1016/0017-9310(84)90001-2.

[32] H.K. Mohanty, Unsteady natural convection in horizontal channels with arbitrary wall temperatures, Int. J. Heat Mass Transf. 22 (1979) 383-388. https://doi.org/10.1016/0017-9310(79)90004-8.

[33] P.K. Muhuri, M.K. Maiti, Free convection oscillatory flow from a horizontal plate, Int. J. Heat Mass Transf. 10 (1967) 717-732. https://doi.org/10.1016/0017-9310(67)90131-7.

[34] V. Sridhar, K. Ramesh, D. Tripathi, V. Vivekanand, Analysis of thermal radiation, Joule heating, and viscous dissipation effects on blood-gold couple stress nanofluid flow driven by electroosmosis, Heat Transfer. 51 (2022) 4080-4101. https://doi.org/10.1002/htj.22490.

[35] D.C. Lu, S. Noreen, S. Waheed, D. Tripathi, Heat transfer applications in curved microchannel driven by electroosmosis and peristaltic pumping, J Mech Med Biol. 22 (2022). https://doi.org/10.1142/s0219519422500300.

[36] K. Vajravelu, P.V. Arunachalam, S. Sreenadh, Unsteady Flow of Two Immiscible Conducting Fluids Between Two Permeable Beds, J. Math. Anal. Appl. 196 (1995) 1105-1116. https://doi.org/10.1006/jmaa.1995.1463.

[37] A. Hibara, M. Tokeshi, K. Uchiyama, H. Hisamoto, T. Kitamori, Integrated Multilayer Flow System on a Microchip, Anal Sci. 17 (2001) 89-93. https://doi.org/10.2116/analsci.17.89.

[38] B.A. Packham, R. Shall, Stratified laminar flow of two immiscible fluids, Math. Proc. Cambridge Philos. Soc. 69 (1971) 443-448. https://doi.org/10.1017/s0305004100046880.

[39] C.R. Faust, Transport of Immiscible Fluids Within and Below the Unsaturated Zone: A Numerical Model, Water Resour. Res. 21 (1985) 587-596. https://doi.org/10.1029/wr021i004p00587.

[40] A.B. Wakale, K. Venkatasubbaiah, K.C. Sahu, A parametric study of buoyancy-driven flow of two-immiscible fluids in a differentially heated inclined channel, Comput Fluids. 117 (2015) 54-61. https://doi.org/10.1016/j.compfluid.2015.04.021.

[41] M.S. Malashetty, J.C. Umavathi, J. Prathap Kumar, Two fluid flow and heat transfer in an inclined channel containing porous and fluid layer, Heat Mass Transf. 40 (2004) 871-876. https://doi.org/10.1007/s00231-003-0492-2.

[42] Y. Abd Elmaboud, Two layers of immiscible fluids in a vertical semi-corrugated channel with heat transfer: Impact of nanoparticles, Results Phys. 9 (2018) 1643-1655. https://doi.org/10.1016/j.rinp.2018.05.008.

[43] Y. Abd Elmaboud, S.I. Abdelsalam, Kh.S. Mekheimer, K. Vafai, Electromagnetic flow for two-layer immiscible fluids, Eng. Sci. Technol. an Int. J. 22 (2019) 237-248. https://doi.org/10.1016/j.jestch.2018.07.018.

[44] SUS Choi, Enhancing thermal conductivity of fluids with nanoparticles. In Developments and Applications of Non-Newtonian Flows,J A. 231(1995)99-105. https://www.osti.gov/servlets/purl/196525

[45] B.C. Rout, S.R. Mishra, T. Thumma, Effect of viscous dissipation on Cu-water and Cu-kerosene nanofluids of axisymmetric radiative squeezing flow, Heat Transfer-Asian Research. 48 (2019) 3039-3054. https://doi.org/10.1002/htj.21529.

[46] R. Hossain, A.K. Azad, Md. Jahid Hasan, M.M. Rahman, Thermophysical properties of Kerosene oil-based CNT nanofluid on unsteady mixed convection with MHD and radiative heat flux, Eng. Sci. Technol. an Int. J. 35 (2022) 101095. https://doi.org/10.1016/j.jestch.2022.101095.

[47] I. Zari, A. Shafiq, T.S. Khan, S. Haq, Marangoni Convective Flow of GO-kerosene- and GO-water-based Casson Nanoliquid Toward a Penetrable Riga Surface, Brazilian J. Phys. 51 (2021) 1747-1762. https://doi.org/10.1007/s13538-021-00922-7.

[48] A.S. Dogonchi, D.D. Ganji, Thermal radiation effect on the Nano-fluid buoyancy flow and heat transfer over a stretching sheet considering Brownian motion, J. Mol. Liq. 223 (2016) 521-527. https://doi.org/10.1016/j.molliq.2016.08.090.

[49] M.M. Bhatti, T. Abbas, M.M. Rashidi, Entropy generation as a practical tool of optimisation for non-Newtonian nanofluid flow through a permeable stretching surface using SLM, J Comput Des Eng. 4 (2016) 21-28. https://doi.org/10.1016/j.jcde.2016.08.004.

[50] J. Akram, N.S. Akbar, D. Tripathi, A Theoretical Investigation on the Heat Transfer Ability of Water-Based Hybrid (Ag–Au) Nanofluids and Ag Nanofluids Flow Driven by Electroosmotic Pumping Through a Microchannel, Arab J Sci Eng. 46 (2021) 2911-2927. https://doi.org/10.1007/s13369-020-05265-0.

[51] E.N. Maraj, I. Zehra, N. SherAkbar, Rotatory flow of MHD $(MoS_2-SiO_2)/H_2O$ hybrid nanofluid in a vertical channel owing to velocity slip and thermal periodic conditions, Colloids Surf. A Physicochem. Eng. Asp. 639, (2022), 128383, https://doi.org/10.1016/j.colsurfa.2022.128383.

[52] Z.-Y. Xie, Y.-J. Jian, F.-Q. Li, Thermal transport of magnetohydrodynamic electroosmotic flow in circular cylindrical microchannels, Int. J. Heat Mass Transf. 119 (2018) 355-364. https://doi.org/10.1016/j.ijheatmasstransfer.2017.11.026.

Declaration of interests

☐ The authors declare that they have no known competing financial interests or personal relationships that could have appeared to influence the work reported in this paper.

☒ The authors declare the following financial interests/personal relationships which may be considered as potential competing interests:

Sara I. Abdelsalam reports travel was provided by Fundación Mujeres Por África. Abdullah Madhi Alsharif reports administrative support was provided by Taif University.